Research Square

Preprints are preliminary reports that have not undergone peer review.
They should not be considered conclusive, used to inform clinical practice,
or referenced by the media as validated information.

Hydrogen production from low-temperature water-driven oxidation of iron

Maxime Durelle
Donostia International Physics Center
Borja Aparicio
Donostia International Physics Center
Smruti Sourav Rout
University of Bremen
Aitor Larrañaga Varga
University of the Basque Country
Wolfgang Bach
University of Bremen
Juan Manuel García-Ruiz
juanma.garciaruiz@gmail.com

Donostia International Physics Center

Article

Keywords:

Posted Date: November 12th, 2026

DOI: https://doi.org/10.21203/rs.3.rs-11432397/v1

License: This work is licensed under a Creative Commons Attribution 4.0 International License.
Read Full License

Additional Declarations: No competing interests reported.

Abstract

Understanding how hydrogen forms through mineral-water reactions is essential for studying Earth's earliest geochemistry and for developing clean energy sources. We experimentally demonstrate that water oxidizes ferrous ions in silica-rich alkaline solutions, producing substantial amounts of molecular hydrogen over a prolonged period of time. We propose a mechanism involving direct precipitation of green rust without any intermediate. This occurs when ferrous and chloride ions are compartmentalized within green-rust/silica double membranes, with continuous water reduction and iron oxidation driving hydrogen generation. At a planetary scale, this pathway may have been as important as serpentinization in providing H_2 essential for prebiotic reaction networks. Furthermore, the reaction we discovered could pave the way for a cost-effective method of producing molecular hydrogen.

Introduction

Molecular hydrogen (H_2) and the reduced chemical environment it induces are essential to prebiotic reactions[1], and H_2 likely fueled Earth's earliest metabolism[2,3]. Loss of H_2 to outer space would have led to rapid oxidation of Early Earth surface environments. A resupply of H_2 by geochemical reactions was therefore essential to keep Earth's oceans and atmosphere reduced during the Hadean, a period during which life likely evolved[4]. Constraining the mechanisms and conditions under which abiotic H_2 is generated is key for reconstructing the redox evolution of Earth's early hydrosphere and atmosphere and for identifying analogous processes on other planetary bodies.

The canonical mechanism for abiotic H_2 production in geological settings is serpentinization of ultramafic rocks. Serpentinization processes are fairly well understood and have been identified as a significant source of geological H_2 throughout Earth's history[5–7]. Other geochemical reactions[7] may have contributed to early planetary H_2 budgets to some extent. Unexplored is the potential of ferrous iron – an abundant constituent of Early Earth oceans – for supplying H_2 to Hadean surface environments.

Ferrous iron was supplied by the venting of hydrothermal fluids to the Early Earth oceans where it may have reacted in various ways. It may have formed siderite or greenalite without getting oxidized[8]. Alternatively, ferrous iron may have been partly oxidized and formed mixed-valency phases such as green rust, a class of Fe^{2+}/Fe^{3+} layered double hydroxides with the general formula $[Fe^{2+}_{(1-x)}Fe^{3+}_x(OH)_2]^{x+}[(x/n)A^{n-}\cdot(m/n)H_2O]^{x-}$. Green rust is known to from metastably under mildly alkaline, Fe-rich, low-oxygen conditions analogous to those inferred for Archean aqueous environments[9,10]. Recent work has begun to implicate green-rust phases in the abiotic reduction of inorganic compounds[11–14], but their role in driving hydrogen generation through coupled iron oxidation and water reduction has not been systematically investigated.

In this study, we report experimental evidence that the oxidation of Fe^{2+} by water in silica-rich, alkaline solutions produces substantial amount of molecular hydrogen over prolonged timescales of reaction.

We propose a mechanistic framework in which ferrous and chloride ions are compartmentalized within green-rust/silica double membranes, structurally coherent interfaces that concentrate redox-active iron phases and sustain the thermodynamic gradients required for continuous water reduction. This reaction pathway may have operated widely in silica- and iron-rich aqueous environments of Early Earth. It could have played a substantial role in supplying H_2 essential for the molecular evolution in prebiotic environments.

Results

Our experimental approach was triggered by the observation that the formation of tubular structures forming by mixing of metal salts with alkaline silica-rich solutions, also known as silica gardens[15], is guided in most cases by bubbling. A degassed sodium silicate solution with a SiO2 concentration of 1.13 mol/kg solution, and a pH value of 11.6 was poured into a sealed vial containing ferrous salts under an N_2 atmosphere (Supplementary fig. S1). White tubular structures began to form immediately. After 10 min, the vertical growth of tubular structures slowed, and after 30 min, these structures began to turn green. At 2h of reaction, all the tubular structures appeared green, and no further color change could be detected (Supplementary fig. S1). The system was allowed to react at room temperature for at least 4 days, after which the gas phase in the headspace was analyzed by gas chromatography. We detected the formation of hydrogen for all Fe(II) salts (Supplementary table S1), reaching a maximum concentration of up to 51,000 ppm with $FeCl_2$ (Supplementary table S2). Water was the sole source of H_2 in our experiment, as reactions were carried under O_2-free condition. Consequently, H_2 was generated through the reduction of water and the oxidation of Fe^{2+} ions.

We found that the main parameters influencing H_2 production in the iron-silica system are the concentration of the sodium silicate solution and the amount of solid iron added. As shown in Fig. 1a, increasing the sodium silicate concentration from 0.06 to 1.13 $mol.kg^{-1}$ (3600 to 67765 ppm) while keeping the mass $FeCl_2$ constant resulted in higher H_2 production. No significant H_2 was produced when [SiO_2] was less than or equal to 0.06 mol.kg-1 (3600 ppm), and therefore, no H_2 was generated in silica-free solutions. Maintaining a silicate concentration of 1.13 $mol.kg^{-1}$ and increasing the amount of iron in the system also resulted in a rise in hydrogen production (Fig. 1B). Two behaviors can be distinguished: up to 9 mg of $FeCl_2$, H_2 production increased proportionally with a constant efficiency (H_2 produced per unit of Fe^{2+}), whereas, after that point, the efficiency started to decline. This decline in H_2 production efficiency is attributed to extensive initial precipitation, which impedes transport between the silicate solution and the unreacted iron within the tubular structures. Temperature and pH had minimal effects on hydrogen production (Supplementary fig. S2).

Hydrogen started to form shortly after the reactants were mixed, and then the rate of H_2 formation decreased constantly (Fig. 1C). However, even after 120 hours, a measurable amount of H_2 continued to be produced, while no changes in the quantity, color, size, or texture of the tubular structures could be observed.

Mineral characterization

Scanning Electron Microscopy with Energy-Dispersive X-ray Spectroscopy (SEM-EDX) mapping of tubular structures extracted from their reactive medium clearly showed a double layer composed of a silica-rich and a metal-rich part that spontaneously form in solution (Fig. 2A–F). The iron-rich inner layer ranged from 2 to 4 µm thick, while the distinct silica outer layer measured 1 to 2.5 µm (Fig. 2A–B). Breaking these tubular structures by stirring the reactive medium did not hinder H_2 production, as a similar amount was generated, as shown in Fig. 2J. This is because stirring the solution did not inhibit the formation of a double layer. Silica gel continuously precipitated around the acidic iron solution to form vesicle-like particles with an iron-rich inner edge and a silica-rich outer edge (Fig. 2G–I). These results suggest that neither the exact shape of these structures (tubes or particles) nor the formation mechanism (buoyancy force in a still solution or constant shell breaking in a stirred solution) strongly affects hydrogen production, as long as the green-rust/silica double membrane compartmentalizes ferrous and chloride ions.

We first examined the products of the oxidation process using ex situ X-ray diffraction (XRD). We aged tubular structures formed in standard experiments (under an N_2 atmosphere) in their sealed vials. Then, Kapton capillaries were filled with the sodium silicate solution and the tubular structures formed at different reaction times, sealed and analyzed by XRD. We found that the only crystalline iron structure formed even after one month was green rust chloride (GR-Cl, Fig. 3A). Green rust is a mixed-valent iron hydroxide with a typical Fe(II)/Fe(III) ratio of 3, featuring a layered structure that alternates between layers of iron hydroxide and disordered layers containing Cl^- ions and water (Supplementary fig. S3).

Thereafter, we performed in situ X-ray diffraction experiments by adding a sodium silicate solution to $FeCl_2$ powder placed inside a Kapton capillary. We analysed by XRD the tubular structures forming in the capillary for up to 120 hours with 5 hours scans. The first signs of crystallinity appeared after 10 hours, with Bragg peaks of green rust chloride (GR-Cl) (Fig. 3B) beginning to grow, reaching a maximum after 25 hours (Fig. 3C). After 50 hours, the intensity of the GR-Cl peaks started to decrease, and they became undetectable after 65 hours. Bragg peaks of akaganeite began to grow after 85 hours and continued to increase until the end of the experiment at 120 hours. The disappearance of GR-Cl before akaganeite formed in this experiment is likely due to limited sensitivity (see supplementary Fig. S4 and Supplementary Discussion 1 for further discussion). The noticeable loss of liquid from the capillary indicates that the reactive medium evaporated and was therefore exposed to air during the prolonged in situ experiment. This process allows oxygen to readily reach green rust, thereby initiating oxidation and forming akaganeite, as observed in previous studies[16–18]. During the whole life of GR-Cl, the d-value of the (003) plane, corresponding to the distance between two iron hydroxide layers in GR-Cl, was decreasing (Fig. 2C). At the formation of the GR-Cl, $d_{GR}^{003} = 8.0$ Å, as expected for hydrated GR-Cl[10]. Over time, d_{GR}^{003} decreases until reaching $d_{GR}^{003} = 7.8$ Å at 50 hours of reaction. It is known that, in a reactive medium rich in Cl^-, green rust progressively enriches in Cl^- and Fe(III)[16]. The Fe^{2+} cation is larger than the Fe^{3+} cation, and the transformation from one to the other leads to contraction of the iron layer

and thus of the overall layered structure[19]. Therefore, our results demonstrate that GR-Cl continued to be oxidized by water after its precipitation.

Discussion

Figure 4 shows a phase diagram of the Fe-O-H-Cl system, illustrating the stability of GR-Cl relative to other possible Fe precipitates. The following four chemical equations may be involved in the production of H_2:

$Fe^{2+} + 2H_2O = Fe(OH)_2 + 2H^+$ (R1)

$4Fe(OH)_2 + Cl^- + H^+ = Fe^{(iii)}Fe^{(ii)}_3(OH)_8Cl + 0.5\ H_2$ (R2)

$4Fe^{2+} + 8H_2O + Cl^- = Fe^{(iii)}Fe^{(ii)}_3(OH)_8Cl + 7H^+ + 0.5\ H_2$ (R3)

$Fe^{2+} + 2H_2O = FeO(OH) + 2H^+ + 0.5\ H_2$ (R4)

R1 followed by R2 were claimed to produce H_2 (Dodd et al.[11], Truong et al.[12]) by the formation and oxidation of iron hydroxide. In our case we found the formation of GR without iron hydroxides as an intermediate phase. Actually, when $Fe(OH)_2$ formed in the silica free experiment, no H_2 was produced. Therefore, we claim that the key reaction in our system is R3.

A reaction pathway is proposed to explain the production of H_2. In the initial segment of the reaction path (A in Fig. 4), proton transfers across the membrane raise the pH inside the tubes from pH 4.5 (FeCl2 saturated solution) to pH 6, and the solution becomes supersaturated with respect to both goethite and GR. Although goethite is the stable phase, the critical supersaturation for nucleation (CSN) is not reached. According to Ostwald's rule[20], the metastable phase will have the lowest CSN, and green rust will precipitates on the walls of the tubular structures before goethite. Because roughly 1/4th of the iron in GR is ferric, its formation leads to oxidation of Fe(II) in solution. Because water is the oxidant, H_2 is produced in the process. Once GR forms, the stoichiometry of R3 indicates that H_2 activity will go up by 14 orders of magnitude when pH increases by one unit within the tubular structure. The continued proton transfer across the double membrane will, hence, drive massive H_2 production (segment B in Fig. 4). This is expected to occur within the exact pH range that Glaab et al.[21] showed prevails inside the tubes for tens of hours (see inset of Fig. 4). The high concentrations of Fe^{2+} and Cl^- inside the Fe-silica tube are essential for GR stability (cf. supplementary fig. S3). Water continues to oxidize iron ions in the GR-Cl structure after formation, producing additional H_2 at a lower rate, consistent with the measurements shown in Fig. 1C. Replacing sodium silicate with a silica-free solution did not lead to compartmentalization (Supplementary fig. S5); therefore, the mineral route shown in Fig. 4 is not feasible. In contrast, amorphous $Fe(OH)_2$ forms without H_2 production (See supplementary material for details). Therefore, in the proposed mechanism, the sole role of silica is to generate the

compartmentalisation that makes the formation of green rust possible via R3, by maintaining a pH between 6 and 7 and a high concentration of both Fe^{2+} and Cl^- in a silica-free environment. We envisage that the reaction R3 can occur and produce H_2 in different systems leading to the same conditions occurring inside the vesicle-like particles described here.

Our results show that hydrogen production by water-driven oxidation of Fe(II) is rapid and efficient. Unexpectedly, a significant amount of H_2 was also produced when air (and not pure N_2) was the headspace gas (Fig. 2J). These results strongly indicate that the oxidation of Fe(II) by water to form GR can outcompete the oxidation of ferrous iron by O_2. The speed of this reaction distinguishes it from the Schikorr reaction, which is often used to study the oxidation of iron by water. In that reaction, Fe^{2+} first forms a $Fe(OH)_2$ precipitate that reacts with water to form magnetite (Fe_3O_4) and H_2[22–24]. However, the oxidation of pure $Fe(OH)_2$ is extremely slow and does not readily produce H_2 even at temperatures close to 100°C[22]. Reardon[23] observed that adding Na_2CO_3, NaCl, or Na_2SO_4 increased H_2 production yield and proposed that these substances act as catalysts in the Schikorr reaction. However, all of these salts are commonly found as counterions in green rust structures and could have contributed to its precipitation. Therefore, the oxidation route we propose (Fe(II) → GR → Fe(III) enriched GR) could be a realistic alternative to the Schikorr reaction. That oxidation route could be important for predicting when and how H_2 is produced, especially in systems such as central boilers[25,26] or radioactive waste containers[27], where any H_2 production could lead to severe structural damage.

A recent study on iron-rich alkaline vent analogs proposed a reaction path involving the oxidation of Fe^{2+} and the formation of H_2. Truong et al.[12] proposed that the Schikorr reaction was responsible for the production of H_2, based on the thermodynamic feasibility of the reaction. However, their experiment produced a large amount of green rust in a system that produces a high concentration of Fe^{2+}, Cl^- and CO_3^{2-} in conditions close to neutral pH for an extended period of time. The production of H_2 could be explained by precipitation and further oxidation of that green rust. Therefore, hydrogen production in these systems would depend not only on a pH gradient but also on the concentrations of Cl^- and CO_3^{2-}, which are necessary for green rust to precipitate.

Dodd et al.[11] also found green rust forming in iron precipitation experiments in silica-bearing solutions. They suggested that iron precipitated as $Fe(OH)_2$ and was subsequently oxidized by water to form green rust, which produced the H_2 they detected in their process. In light of our experimental results, an alternative interpretation for their H_2 production is the direct formation of green rust from Fe^{2+} ions. Once again, this underscores the importance of the counterion, in this case sulfate, which is critical for green rust formation and H_2 production.

Our results strengthen the idea that green rust and the production of H_2 may have played an important role in the early ocean[11,12,28–30]. We further investigated this by performing experiments that mimicked the water of Aqua de Ney spring, a naturally alkaline water with a high silica content (4296 ppm), whose chemistry originates from serpentinization reaction and could therefore be considered a good model for

the Hadean hydrosphere[31–33] (see method section). We found that when a sodium silicate solution with alkalinity corrected to fit the one of Aqua de Ney water is allowed to react with an iron(II) salt not only does it lead to the formation of tubular structures (as actual Aqua de Ney water does[32]), but also produces a substantial amount of H_2 (Fig. 1A). The lower the concentration of CO_3^{2-} in the sodium silicate solution, the higher the production of H_2. The Hadean ocean likely had very high concentrations of Fe and silica, but exceedingly low concentrations of carbonate ions[31,34].

We suggest that copious amounts of H_2 were produced during water-driven iron oxidation and GR formation. This H_2 production could have taken place at sites of hydrothermal venting by two mechanisms: (i) slow seepage of iron-bearing solutions and growth of tubular structures at the seafloor, and (ii) vigorous discharge of very Fe-rich, high-temperature vent fluids and formation of spherical iron/silica double membrane particles upon mixing with seawater that get dispersed over long distances in the Hadean ocean. The overall hydrogen production from Fe(ii) oxidation by water could have been as high as 40 mmol per kg vent fluid, if all of the dissolved iron (80 mmol/kg [35]) were oxidized by this reaction sequence. This H_2 production would come in addition to the H_2 derived from deep-seated serpentinization reaction and would be of similar magnitude, given that fluid venting from modern serpentinization systems has tens of mmoles of H_2 dissolved. Our findings therefore amplify the role of hydrothermal venting as an essential source of H_2 to the early oceans and atmosphere. Our results suggest that the substantial amount of H_2 present in early Earth's atmosphere may have originated from the formation of green rust within self-assembled silica structures, rather than solely from serpentinization (supplementary table S4).

The oxidation path we propose is a new route for H_2 production using among the most common and cheapest compounds on Earth (iron and silica). The reaction occurs spontaneously at room temperature and pressure, requires no noble-metal catalysts, and does not produce CO_2. Given that the maximum theoretical yield of the reaction is 1 mole of H_2 per 2 moles of Fe^{2+}, this method could enable cheap, large-scale production of green hydrogen[36].

Materials and Methods

Experiments

Macroscopic iron-silica garden structures were grown by adding a sodium silicate solution to particles of different metallic salts, as shown in Table I. The experiments were conducted in a 12 mL borosilicate glass vial equipped with a screw cap and a PTFE septum. 70 mg of the metallic salt was added to the vials under ambient conditions (Fig. 1). The vials were flame-dried to remove residual moisture and ensure a clean internal surface. They were immediately connected to a Schlenk line and evacuated under dynamic vacuum for 10 minutes to thoroughly remove atmospheric oxygen. The internal atmosphere was then replaced with nitrogen. This cycle of evacuation and inert gas exchange was repeated twice more to establish strictly anaerobic conditions, preventing premature oxidation of the metallic salts. A

sodium silicate solution was prepared by diluting commercial sodium silicate 1:4 (v:v) in deionized water. The final SiO2 concentration of this standard solution was 0.88 mol/kg(sol), the [Na]/[Si] ratio was 0.78, and the pH was 11.6. For experiment carried at controlled pH, the pH was adjusted at the desired value using a 1 M NaOH solution. The final solution was freshly prepared and degassed by three freeze–pump–thaw cycles to remove atmospheric gases. To maintain an inert environment, 8.0 mL of the degassed sodium silicate solution was added to the vial using a nitrogen-flushed syringe, ensuring minimal disturbance to the anaerobic conditions. Immediately after addition, structures began to form. The system was then sealed and left undisturbed at room temperature or in a furnace at a chosen temperature (between 50 to 90 ºC) for at least 96 hours (4 days) to allow full development of the mineral structures and potential generation of gaseous species. Additional tests were conducted using different salts shown in supplementary table S1.

In addition, a series of experiments was conducted with a sodium silicate solution under conditions that mimic those of the Aqua de Ney spring. All other parameters were kept constant. The first reaction was performed using a sodium silicate solution with the same pH, silicate and carbonate concentrations as those reported for Aqua de Ney(31): 12.2, 4200 ppm and 4000 ppm, respectively. A second reaction was performed using a sodium silicate solution in which the carbonate ions were replaced with twice the amount of NaOH to maintain alkalinity similar to that found in these waters.

Gas measurements

The gases from the experiments were analyzed using gas chromatography at the University of Bremen and at Isolab. In th Universit of Bremen, H_2 concentrations were determined with a 7820A Agilent gas chromatograph (GC). First, a syringe headspace extraction was conducted, and the H_2 in the headspace gas was quantified using a thermal conductivity detector (TCD) adapted from Klose et al. (2021), operating at 200–250°C. The GC is fitted with a Molsieve 60/80 column (Sigma-Aldrich, St. Louis, MO) with a 1 mL loop volume and uses N_2 as the carrier gas at 70°C. The analytical uncertainties (2σ) are less than ± 2% for H_2. The setup was calibrated with a standard reference gas containing 1 vol% H_2 in N_2. For each sample, 2–3 extractions and measurements were performed at different times, ranging from 15 minutes to 48 hours, to assess H_2 solubility in the sample fluid and to confirm analysis precision. In Isolab, H_2, O_2, Ar, N_2, CO and methane concentrations were determined with a 7890A Agilent GC equipped with a 25m, 0.32mm molsieve 5A column (Agilent) and a TCD detector. Hydrocarbons and CO2 were analyzed on an Agilent 7890B GC equipped with a 50m, 0.32mm Porabond-Q column (Agilent), coupled to a TCD detector (for CO_2 and H_2S) and a 30m 0.32mm Gaspro column (Agilent), coupled to an FID detector (for hydrocarbons). Both GCs are equipped with a heated valve for injection of the samples and on both GCs, Helium is used as carrier gas. One complete composition is calculated from the results of the three detectors. Detector responses are calibrated several times a day using various reference standards.

X-Ray diffraction

To confirm that the transformation described in this X-ray experiment also occurs in a real sample, an experiment was conducted in a Kapton capillary. Some grains of $FeCl_2$ powder were deposited in the middle of the capillary before it was filled with a sodium silicate solution. Small tubular structures quickly formed around the $FeCl_2$ grains and the X-ray beam was then centered on these structures, and diffraction patterns were recorded for 5 hours each. X-ray measurements were obtained by using a Rigaku Smartlab automatic diffractometer operating at 40 kV and 50 mA. The 2θ scans in transmission mode were obtained with parallel beam configuration (CBO), capillary attachment head, Knife-edge, Cu-Kα filter, automatic attenuator and 1-D DteX250 detector. The diffraction data were collected with an 8 to 38º step size of 0.02º at 0.1–0.5º/min scan speed.

All diffraction patterns have been processed using custom Python code. The background was estimated using an ARPLS (Asymmetrically Weighted Penalised Least Squares) algorithm and then subtracted from the data prior to integration using Simpson's rule. The positions of the peaks and the full width at half maximum (FWHM, β_{sample}) were computed for the (003), (006), (012) and (015) reflections of green rust and the (110), (211) and (310) reflections of akageneite by fitting a pseudo-Voigt profile to the background-subtracted data using a least-squares method.

Thermodynamic calculations

Geochemist's Workbench module Act2 was employed to construct the phase diagram in Fig. 4, using the thermo.com.V8. R6 + database. Thermodynamically stable phases in the Fe-Si-O-H system (minnesotaite, hematite, magnetite) were suppressed. The stability field of green rust (GR) is based on a ΔfGo value of -2145 kJ/mol for GR-Cl (Nacib et al., 2016) and a ΔrGo value of -172.48 kJ/mol for the reaction $Fe^{(iii)}Fe^{(ii)}_3(OH)_8Cl + 8H^+ = 3Fe^{2+} + Fe^{3+} + Cl^- + 8H_2O$ using ΔfGo values of -90.5, -17.24, -131.30, and − 237.18 kJ/mol for Fe^{2+}, Fe^{3+}, Cl^-, and H_2O, respectively. The corresponding Log K (25°C) value of 30.23 for GR-Cl dissolution was added to the database.

Scanning electron microscopy and EDX analysis

Samples for SEM examination were prepared by adding a sodium silicate solution to $FeCl_2$ powder in a 7 mL vial that was left open to the air. After 30 minutes, some of the tubes formed in the reaction mixture were collected using a micro spatula, washed in Milli-Q water and placed on a carbon tape stick attached to an SEM pin. They were then quickly placed in a vacuum oven at room temperature and at approximately 6 mPa for at least 30 minutes to dry while avoiding oxidation. SEM images were recorded using a JSM-IT800HL (JEOL) equipped with a Field Emission Gun using an acceleration voltage of 7 kV, an in-chamber Scintillator Backscattered Electron Detector, and an Everhart–Thornley detector with a 300 V bias. The SEM-EDS images were recorded using a window-less, 100 mm^2 sized EDS detector mounted extra close to the sample at a 35º angle optimised to work at an acceleration voltage of 7 kV.

Declarations

Competing Interest Statement:

Authors declare that they have no competing interests.

Funding:

This work is part of the PROTOS project, which has received funding from the European Research Council (ERC) (Grant Agreement No. 101118811). It is funded by the European Union. However, the views and opinions expressed are those of the author(s) only and do not necessarily reflect those of the European Union or the European Research Council Executive Agency. Neither the European Union nor the granting authority can be held responsible for them.

Author Contribution

Conceptualization: JMGR, WB; Chemical experiments: BA, MD, JMGR; Hydrogen measurement: SSR; XRD experiment: ALV, MD, JMGR; Data analysis: MD, JMGR, WB; Funding acquisition: JMGR, WB; Writing – original draft: JMGR, MD; Writing – review & editing: JMGR, MD, WB

Acknowledgement

We acknowledge Marco Moller from CIC Biomagune for help with scanning electron microscopy and Dr. Jorge Vago from the European Space Agency for critical reading of the manuscript and useful discussions. We acknowledge the European Research Council (ERC), which funded this work (Grant Agreement No. 101118811). However, the views and opinions expressed are those of the author(s) only and do not necessarily reflect those of the European Union or the European Research Council Executive Agency. Neither the European Union nor the granting authority can be held responsible for them.

Data Availability

The authors confirm that the data supporting the findings of this study are available within the article and its supplementary materials.

References

1. Miller, S. L. A Production of Amino Acids Under Possible Primitive Earth Conditions. *Science* **117**, 528–529 (1953).

2. Weiss, M. C. et al. The physiology and habitat of the last universal common ancestor. *Nat. Microbiol.* **1**, 16116 (2016).
3. Martin, W., Baross, J., Kelley, D. & Russell, M. J. Hydrothermal vents and the origin of life. *Nat. Rev. Microbiol.* **6**, 805–814 (2008).
4. Preiner, M. et al. A hydrogen-dependent geochemical analogue of primordial carbon and energy metabolism. *Nat. Ecol. Evol.* **4**, 534–542 (2020).
5. Sleep, N. H., Meibom, A., Fridriksson, T., Coleman, R. G. & Bird, D. K. H_2 -rich fluids from serpentinization: Geochemical and biotic implications. *Proc. Natl. Acad. Sci. U.S.A.* 101, 12818–12823 (2004).
6. Tamblyn, R. & Hermann, J. Geological evidence for high H2 production from komatiites in the Archaean. *Nat. Geosci.* **16**, 1194–1199 (2023).
7. Klein, F., Tarnas, J. D. & Bach, W. Abiotic Sources of Molecular Hydrogen on Earth. *Elements* **16**, 19–24 (2020).
8. Tosca, N. J. & Tutolo, B. M. Hydrothermal vent fluid-seawater mixing and the origins of Archean iron formation. *Geochim. Cosmochim. Acta*. **352**, 51–68 (2023).
9. Génin, J. M. R., Ruby, C., Géhin, A. & Refait, P. Synthesis of green rusts by oxidation of Fe(OH)2, their products of oxidation and reduction of ferric oxyhydroxides; E h –pH Pourbaix diagrams. *Comptes Rendus Géoscience*. **338**, 433–446 (2006).
10. Cornell, R. M. & Schwertmann, U. *The Iron Oxides: Structure, Properties, Reactions, Occurrences and Uses* (Wiley-VCH, 2006).
11. Dodd, M. S. et al. Abiotic anoxic iron oxidation, formation of Archean banded iron formations, and the oxidation of early Earth. *Earth Planet. Sci. Lett.* **584**, 117469 (2022).
12. Truong, C. et al. Fe2 + disproportionation within iron-rich alkaline vent analogues reveals proto-bioenergetic systems. *Nat. Commun.* **16**, 10682 (2025).
13. Lee, S., Wang, C., Chakrapani, V. & Green Rust A Potent Reductant for Unassisted Conversion of CO to Multicarbon Liquid Products. *J. Phys. Chem. C*. **128**, 15778–15784 (2024).
14. Ezz-Elregal, E. E. M. et al. A Catalyst for Sodium Borohydride Dehydrogenation Based on a Mixed-Valent Iron Hydroxide Platform. *ACS Catal.* **15**, 12269–12280 (2025).
15. Barge, L. M. et al. From Chemical Gardens to Chemobrionics. *Chem. Rev.* **115**, 8652–8703 (2015).
16. Refait, P., Abdelmoula, M. & GÉnin, J. M. R. Mechanisms of formation and structure of green rust one in aqueous corrosion of iron in the presence of chloride ions. *Corros. Sci.* **40**, 1547–1560 (1998).
17. Nagata, F., Inoue, K., Shinoda, K. & Suzuki, S. Characterization of Formation and Oxidation of Green Rust (Cl–) Suspension. *ISIJ Int.* **49**, 1730–1735 (2009).
18. Refait, P., Benali, O., Abdelmoula, M. & Génin, J. M. R. Formation of 'ferric green rust' and/or ferrihydrite by fast oxidation of iron(II–III) hydroxychloride green rust. *Corros. Sci.* **45**, 2435–2449 (2003).

19. Wang, X. et al. Effects of Mn or Al incorporation on the structure, composition, and As(III) adsorption of oxidized green rust. *Chem. Geol.* **611**, 121124 (2022).
20. Cardew, P. T. Ostwald Rule of StagesMyth or Reality? *Crystal Growth Design*. **23**, 3958–3969 (2023).
21. Glaab, F., Rieder, J., García-Ruiz, J. M., Kunz, W. & Kellermeier, M. Diffusion and precipitation processes in iron-based silica gardens. *Phys. Chem. Chem. Phys.* **18**, 24850–24858 (2016).
22. Evans, U. R. & Wanklyn, J. N. Evolution of Hydrogen from Ferrous Hydroxide. *Nature* **162**, 27–28 (1948).
23. Reardon, E. J. Anaerobic Corrosion of Granular Iron: Measurement and Interpretation of Hydrogen Evolution Rates. *Environ. Sci. Technol.* **29**, 2936–2945 (1995).
24. Shipko, F. J. & Douglas, D. L. Stability of Ferrous Hydroxide Precipitates. *J. Phys. Chem.* **60**, 1519–1523 (1956).
25. McEnaney, B. & Smith, D. C. Corrosion of a cast iron boiler in a model central heating system. *Corros. Sci.* **18**, 591–603 (1978).
26. Ichihara, T., Koike, R., Watanabe, Y., Amano, Y. & Machida, M. Hydrogen damage in a power boiler: Correlations between damage distribution and thermal-hydraulic properties. *Eng. Fail. Anal.* **146**, 107120 (2023).
27. Ortiz, L., Volckaert, G. & Mallants, D. Gas generation and migration in Boom Clay, a potential host rock formation for nuclear waste storage. *Eng. Geol.* **64**, 287–296 (2002).
28. Tosca, N. J., Jiang, C. Z. & Tutolo, B. M. The Precambrian Greenalite Factory. *Elements* 21, 191–196 (2025).
29. Tostevin, R. & Sevgen, S. The role of Fe(II)-silicate gel in the generation of Archean and Paleoproterozoic chert. *Geology* **52**, 706–711 (2024).
30. Halevy, I., Alesker, M., Schuster, E. M., Popovitz-Biro, R. & Feldman, Y. A key role for green rust in the Precambrian oceans and the genesis of iron formations. *Nat. Geosci.* **10**, 135–139 (2017).
31. García-Ruiz, J. M., Van Zuilen, M. A. & Bach, W. Mineral self-organization on a lifeless planet. *Phys. Life Rev.* **34–35**, 62–82 (2020).
32. García-Ruiz, J. M., Nakouzi, E., Kotopoulou, E., Tamborrino, L. & Steinbock, O. Biomimetic mineral self-organization from silica-rich spring waters. *Sci. Adv.* **3**, e1602285 (2017).
33. Cook, M. C. et al. A Geochemical Comparison of Three Terrestrial Sites of Serpentinization: The Tablelands, the Cedars, and Aqua de Ney. *JGR Biogeosciences* 126, e2021JG006316 (2021).
34. Moldogazieva, N. T., Terentiev, A. A., Mokhosoev, I. M. & Astakhov, D. V. Redox chemistry of early Earth and the origin of life. *Commun. Chem.* **9**, 143 (2026).
35. Kump, L. R. & Seyfried, W. E. Hydrothermal Fe fluxes during the Precambrian: Effect of low oceanic sulfate concentrations and low hydrostatic pressure on the composition of black smokers. *Earth Planet. Sci. Lett.* **235**, 654–662 (2005).
36. García-Ruiz, J. M., Durelle, M., Aparicio, B. & Blanco, A. Method for producing hydrogen. (2026).

Figures

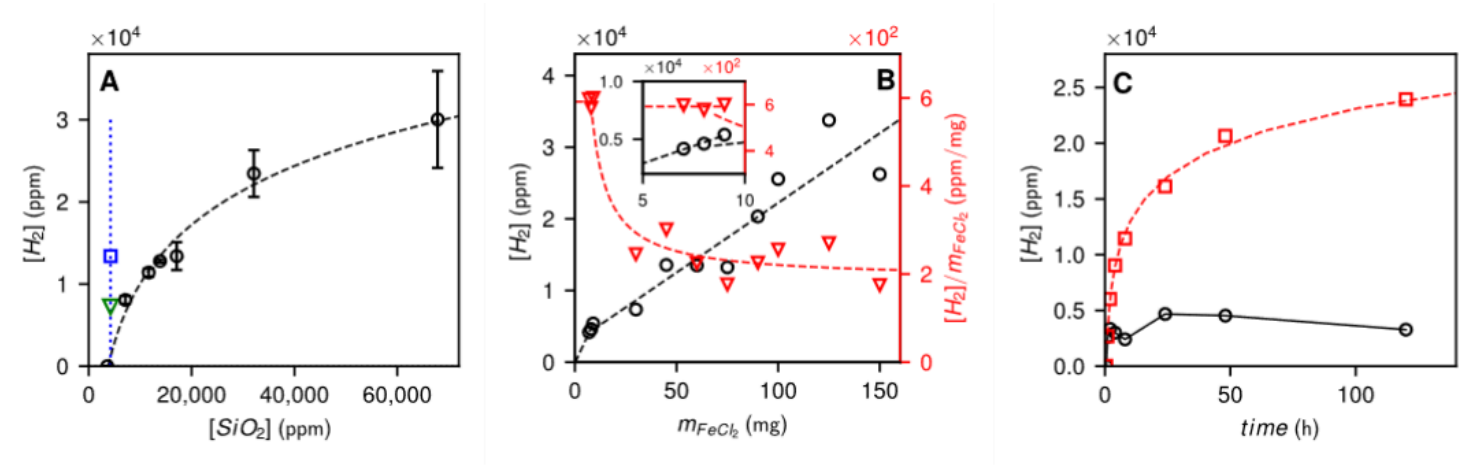


Figure 1

Hydrogen production in the iron silica system H_2 concentration measured in the headspace of the reactive medium (5.6 mL). (**A**) H_2 production versus silicate concentration. The black dashed line is a fitted, shifted logarithmic trend. The blue dotted line indicates the silicate concentration in Aqua de Ney spring (4236 ppm). The blue square shows H_2 production in a medium with the alkalinity similar to Aqua de Ney, and the green triangle shows H_2 production at the pH and carbonate levels of Aqua de Ney. (**B**) H_2 production versus the mass of solid iron chloride in the reactive medium. The dashed lines are fitted trends (linear or inverse-proportional), with two different trends fitted using the first three iron mass values and the remaining data. (**C**) H_2production versus time. Black circles represent the measured values obtained by extracting the gas phase above the reactive medium at specific reaction times. Red squares show the cumulative values represented by the black circles.

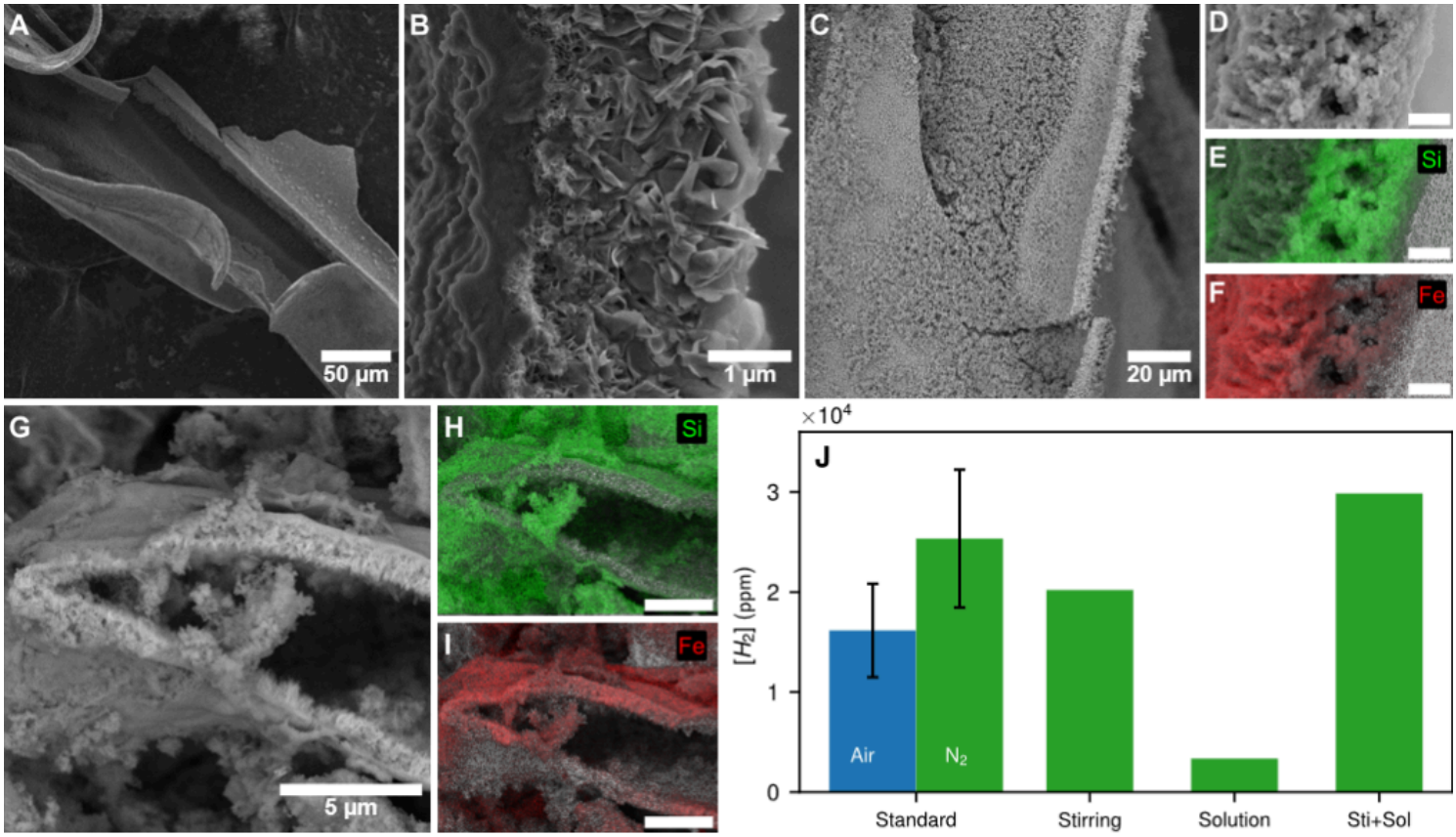


Figure 2

Compartmentalization and H2 production in the iron-silica system (**A**) SEM secondary electron image of a tubular structure formed after adding a sodium silicate solution to $FeCl_2$ particles and (**B**) magnification on a cross section of a wall of that tubular structure. (**C**) Backscattered electron images of a broken tubular structure and (**D**-**F**) SEM-EDX mapping of iron and silicon on the cross section of the wall of the tubular structure. (**G**) SEM backscattered electron images of structures formed when a silicate solution is added to $FeCl_2$ particles under strong agitation. Vesicular structures are formed with distinct double-layer walls. (**H**-**I**) SEM-EDX mapping of Fe and Si on the walls of the vesicular structure. (**J**) H_2 concentration produced in the headspace of the iron-silica system in different conditions. All the green-colored bars represent experiments conducted under an N_2 atmosphere after bubbling N_2 through the sodium silicate solution. The scale bar in figures **D**–**F** is 2 µm, and in figures **H**–**I**, 5 µm.

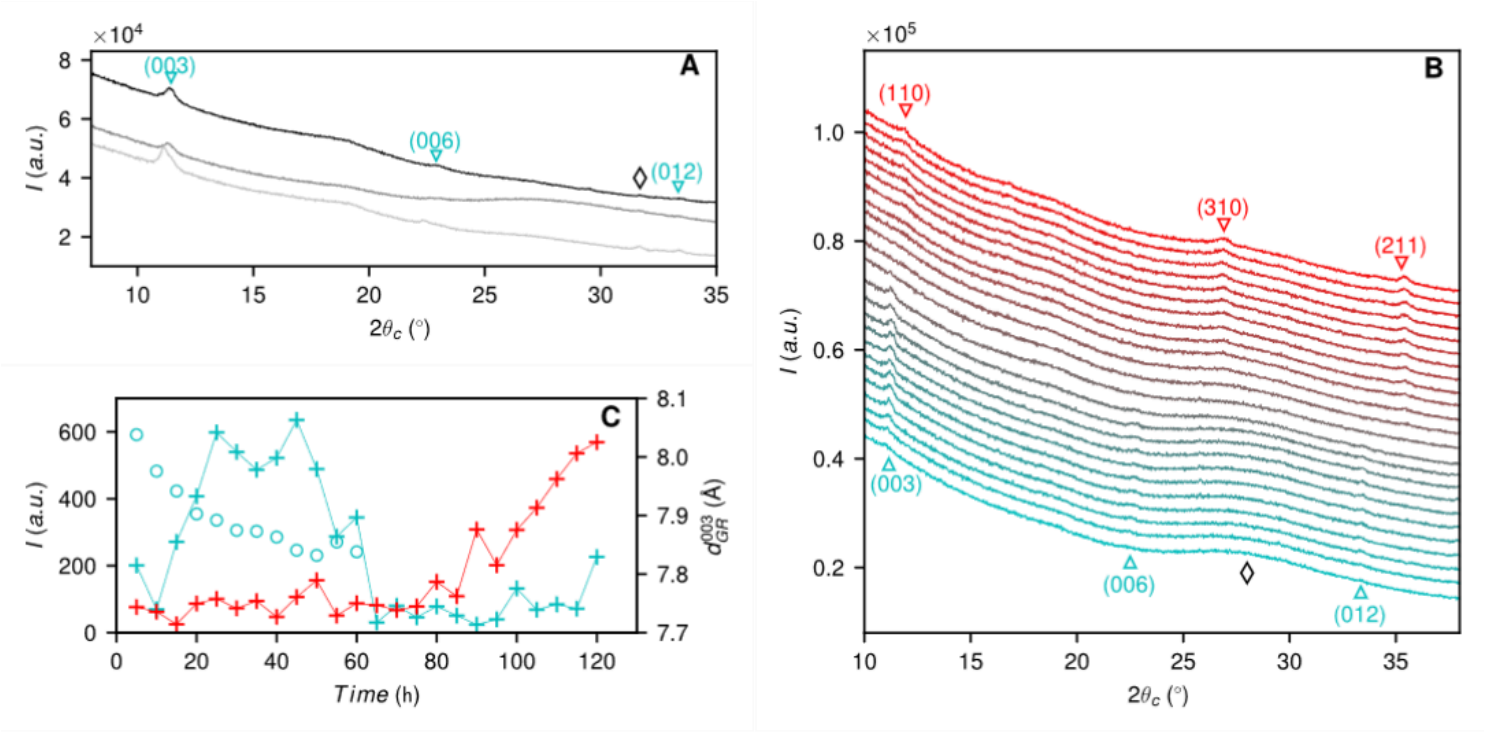


Figure 3

Mineral evolution of the structures formed in the iron-silica system. (**A**) X-ray diffraction pattern of structures formed in the iron-silica system kept under a N_2 atmosphere for (light grey) 5 days, (dark grey) 12 days, and (black) 25 days. Each pattern has been shifted along the Y-axis for clarity. The black diamond indicates the most intense Bragg peak of NaCl, while the cyan triangles indicate the Bragg peak of green rust and the Miller indices of the associated plane. (**B**) Time development of the X-ray diffraction pattern of the reaction products of a sodium silicate solution poured onto a $FeCl_2$ powder inside a Kapton capillary. Each pattern has been shifted along the Y-axis for clarity. The lowest cyan pattern (corresponding to GR-Cl) is after 5 hours of the reaction, and the highest red pattern (corresponding to akaganeite) is after 120 hours. Each pattern is separated by 5 hours. (**C**) Cyan and red crosses: intensity of the Bragg peaks versus time; circles: d^{003} of the GR-Cl as calculated by its peak position using the Bragg equation.

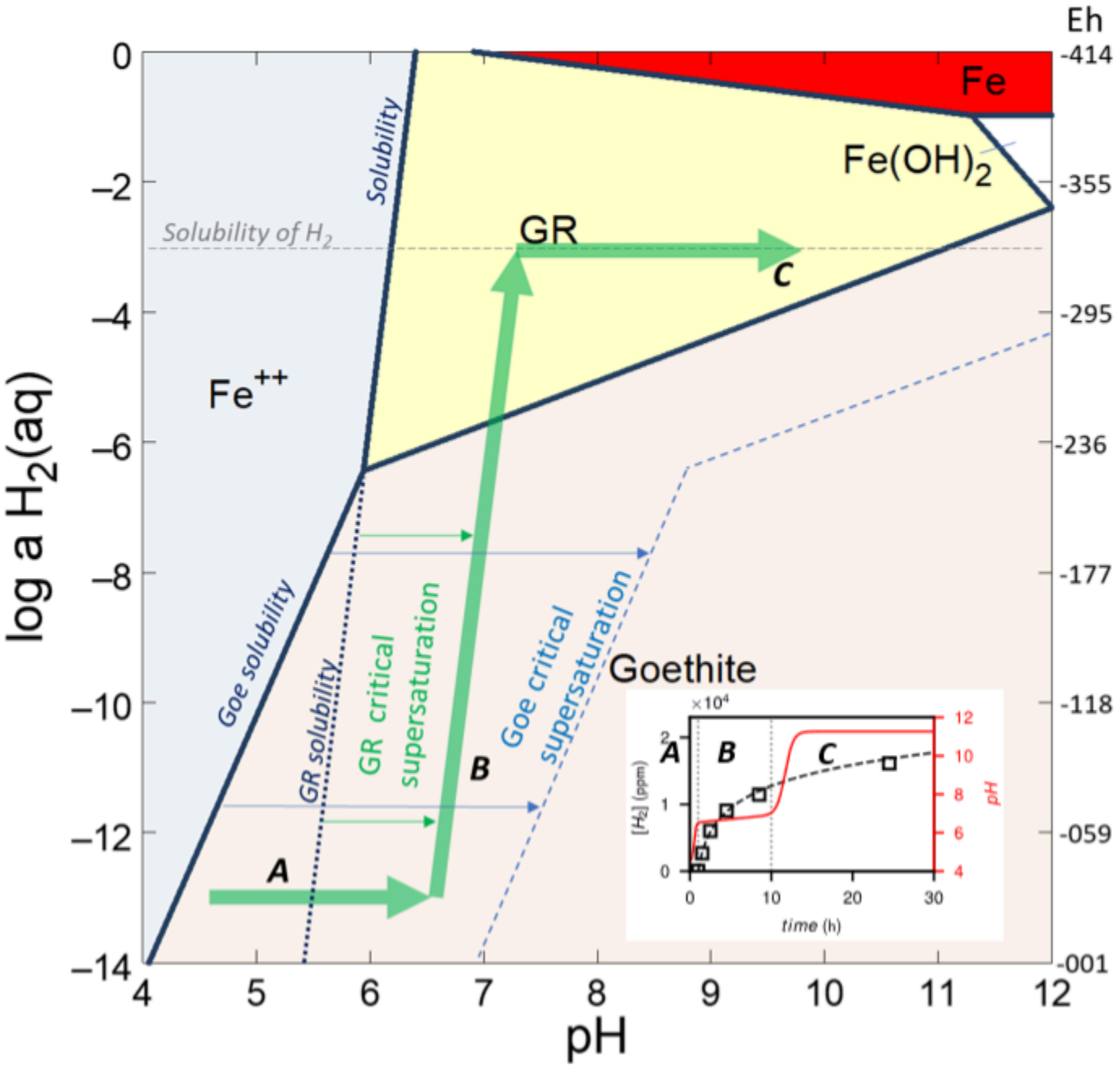


Figure 4

Phase diagram for the system Fe-O-H-Cl. For [Fe], [Cl]≈ 1 mol/kg. The second y-axis shows the Eh values at pH 7 for the corresponding dissolved H2 activities. The steep phase boundary indicates the equilibrium position for R3. The boundary between Fe^{2+} and any solid is its solubility, which can be calculated outside of its thermodynamic predominance field by extending its boundary (dotted line). 'Critical supersaturation for nucleation' denotes the boundary at which the waiting time for nucleation is zero. Also shown is the proposed reaction pathway explaining the production of H_2 via the formation of GR. A: Starting conditions are a pH of 4.5. No solid forms form before path A reaches the critical supersaturation of GR. B: Green rust formation proceeds. An increase in pH driven by proton transfer across the double membrane will cause copious H_2 production. When the solubility of H_2 is reached (B')

the solution begins to degas at a constant pH until the GR has fully precipitated (see inset). C: Once all the GR is formed, pH inside the tube increases by diffusion of HO^- through the double membrane, allowing the enrichment of GR in Fe(III), with continuous production of H_2.

Supplementary Files

This is a list of supplementary files associated with this preprint. Click to download.

- 261001drafth2prodscirepSI2.docx